Asphaltene Adsorption onto Self-Assembled Monolayers of Mixed Aromatic and Aliphatic Trichlorosilanes

Salomon Turgman-Cohen,[1] Matthew B. Smith,[1] Daniel A. Fischer,[2] Peter K. Kilpatrick,[1,†] and Jan Genzer[1,*]

[1] Department of Chemical & Biomolecular Engineering

North Carolina State University

Raleigh, North Carolina 27695-7905

[2] Ceramics Division

National Institute of Standards and Technology

Gaithersburg, Maryland 20899

* Jan_Genzer@ncsu.edu

† Peter.Kilpatrick@nd.edu; Present address: Department of Chemical & Biomolecular Engineering, University of Notre Dame, Notre Dame, Indiana 46656

Abstract

The adsorption of asphaltenes onto flat solid surfaces modified with mixed self-assembled monolayers (SAMs) of aliphatic and aromatic trichlorosilanes with varying wettabilities, aromaticities, and thicknesses is tested. The mixed SAMs are characterized by means of contact angle to assess hydrophobicity and molecular and chemical uniformity, spectroscopic ellipsometry to measure the thickness of the films, and near edge x-ray absorption fine structure (NEXAFS) spectroscopy to assess chemical and molecular composition. The molecular characteristics of the adsorbed asphaltene layer and the extent of asphaltene adsorption are determined using NEXAFS and spectroscopic ellipsometry, respectively. The SAMs are formed by depositing phenyl-, phenethyl-, butyl- and octadecyl- trichlorosilanes from toluene solutions onto silica-coated substrates; the chemical composition and the wettability of the SAM surface is tuned systematically by varying the trichlorosilane composition in the deposition solutions. The adsorption of asphaltenes on the substrates does not correlate strongly with the SAM chemical composition. Instead, the extent of asphaltene adsorption decreases with increasing SAM thickness. This observation suggests that the leading interaction governing the adsorption of asphaltenes is their interaction with the polar silica substrate and that the chemical composition of the SAM is of secondary importance.

Introduction

The fouling of pipes and other solid substrates due to the deposition of insoluble organic compounds from petroleum represents a costly problem facing today's oil industry.[1,2] Among these low solubility organics, asphaltenes are known to play a key role in fouling due to their high affinity to various metal and oxide surfaces.[3-9] Asphaltenes constitute chemically- and structurally-heterogeneous organic molecules that possess high degrees of aromaticity and polarity, relatively high molecular weights (ca. 400-2,000 Da), and have a tendency to form supramolecular aggregates in solution. Asphaltenes are a solubility class of molecules defined as the crude oil fraction insoluble in a low boiling paraffinic solvent (n-pentane or n-heptane) but soluble in aromatic solvents, such as toluene or benzene.[10]

The adsorption of asphaltenes onto solid surfaces has been studied using a variety of experimental methods, including, contact angle measurements,[11,12] atomic force microscopy (AFM),[12-14] photothermal surface deformation (PSD),[8,15-17] Fourier transform infrared spectroscopy (FTIR),[14] quartz crystal microbalance gravimetry (QCM),[6,9,18] x-ray photoelectron spectroscopy (XPS),[7] and ellipsometry.[19] To this end, Acevedo *et al.*[8,16,17] reported on the kinetics of asphaltene adsorption by measuring the optical absorption of dilute asphaltene solutions in contact with silica plates. The authors also used PSD to establish adsorption isotherms on silica plates after 18, 48, and 96 hours of asphaltene adsorption. The authors reported that even at high dilutions asphaltenes adsorbed to silica plates as multilayered deposits. Acevedo and coworkers attributed this multilayered adsorption of asphaltenes to strong asphaltene-asphaltene interactions in solution that resulted in the formation of supramolecular aggregates, which adsorbed onto surfaces. Asphaltenes possess high refractive indices and thus

produce opaque solutions even at low concentrations; optical absorption experiments therefore require accurate dilution procedures in order to monitor the adsorption of asphaltenes. In this respect, QCM studies carried out by several groups[6,9,18] are of high importance because QCM, not being affected by the solution transparency, allows for direct adsorption measurement in a wide range of asphaltene solution concentrations. By utilizing QCM Ekholm *et al.*[18] and Dudášová *et al.*[6] monitored asphaltene adsorption onto a variety of hydrophilic surfaces. Their results revealed that asphaltene adsorption from toluene solution onto hydrophilic surfaces resulted in the adsorption of asphaltene aggregates and the formation of multilayers. The researchers noted that the extent of asphaltene adsorption was governed by the solvent quality, the concentration of asphaltenes in solution, and the chemistry of the asphaltenes, while the exact nature of the hydrophilic surface onto which the asphaltenes are adsorbed played only a minor role. Xie and Karan[9] utilized QCM to monitor the kinetics of asphaltene adsorption onto gold-coated QCM crystals. The authors argued that asphaltenes adsorbed very fast initially, after which they continued adsorbing at a slower rate with no upper limit within the timeframe of the experiments. Labrador *et al.*[19] employed null ellipsometry to monitor the adsorption of asphaltenes onto glass surfaces after 24 and 48 hours of asphaltene adsorption. The results of Labrador and coworkers supported earlier experimental evidence indicating that strong asphaltene-asphaltene interactions contributed to the formation of thick multilayers on substrates.

While most of the research pertaining to asphaltene adsorption onto solid surfaces has been carried out on hydrophilic metal oxide, metallic or glass substrates, very little work has been done on chemically-modified substrates. Hannisdal *et al.*[20] studied the stabilizing power of silica particles on water in oil and oil in water emulsions. While the main focus of their study centered on the stability of asphaltenic emulsions, Hannisdal and coworkers provided an

important insight into the adsorption of asphaltenes onto silica particles of varying wettabilities. In their work, commercially available neat silica particles and particles modified with 2-methacryl oxypropyl trimethoxysilane, polydimethyl siloxane, and dimethyl dichlorosilane were exposed to asphaltene solutions. The authors determined visually that hydrophilic particles appeared darker than hydrophobic ones, indicating that they adsorbed a higher amount of asphaltenes. This observation was further verified with near-infrared spectroscopy by monitoring the intensity of the stretching vibration of methylene groups (2924 cm^{-1}), which provides a relative measure of the hydrocarbon content present on the silica surface. These results confirmed that the amount of asphaltenes adsorbed decreased with increasing hydrophobicity of the particles. In spite of offering important insight into the effect of the hydrophobicity of the substrate on asphaltene adsorption, Hannisdal's *et al.* studies were limited to only a few discrete surfaces. In order to firmly establish the role of hydrophobicity on asphaltene adsorption, one needs to methodically vary the surface energy of the substrate. In this work, we alter systematically the surface energy of the substrate by depositing self-assembled monolayers (SAMs) with gradually varying chemical composition and study the effect of the substrate surface energy on asphaltene adsorption.

SAMs represent an important tool for engineering surfaces through the modification of their physico-chemical properties.[21] Since their introduction in the 1980's by Sagiv and co-workers,[22-28] organosilanes on silica have been among the most widely-used methods for production of well-organized SAMs. Trichlorosilane-based SAMs exhibit great chemical and physical stability due to the reaction of the silane head-group with the silica substrate and subsequent cross-linking among the SAM-forming molecules, leading to the formation of a covalently bound polysiloxane network.[22,29,30] This network endows organosilane-based SAMs

with much higher stability relative to other SAMs, *e.g.*, those formed by assembling thiol-based moieties on noble metal surfaces. Smith *et al.* studied the formation of SAMs by competitive adsorption of aromatic and aliphatic trichlorosilanes from the liquid phase.[31] Using near-edge x-ray absorption fine structure (NEXAFS) spectroscopy and contact angle measurements, Smith and coworkers demonstrated that mixed SAMs with tuned composition can be reproducibly formed by such a deposition method. By varying the ratio of the aromatic to the aliphatic components in the deposition organosilane solutions, the authors engineered SAMs with fine-tuned wettabilities and aromaticities.

In this work, we report on asphaltene adsorption on mixed SAMs. By tailoring the degree of aromaticity and wettability of the SAMs, we hoped to systematically investigate the substrate propensity towards the adsorption of asphaltenes, which are known to contain aromatic cores and aliphatic chains. Specifically, by varying the content of the phenyl- or alkyl- based organosilanes and their packing densities in the SAMs we intended to tune systematically the affinity of the asphaltene molecules to the solid substrate. The structural and physical properties of the SAMs will be characterized with contact angle, spectroscopic ellipsometry, and NEXAFS measurements. The properties of the adsorbed asphaltenes and the extent of adsorption will be characterized with NEXAFS spectroscopy and spectroscopic ellipsometry, respectively. As will be documented later in this paper, the wettability of the substrate does not seem to be the primary factor governing the adsorption of asphaltenes to such mixed SAMs. Instead, we will demonstrate that the thickness of the SAM coating appears to be the leading parameter that regulates the amount of asphaltene adsorption. This leads to the conclusion that the SAM coating acts primarily as a buffer layer regulating the strength of the interaction between asphaltene molecules and the underlying polar silica substrate.

Materials and methods

Materials. n-butyltrichlorosilane (BTS), n-octadecyltrichlorosilane (ODTS), n-phenyltrichlorosilane (PTS) and n-phenethyltrichlorosilane (PETS) were purchased from Gelest, Inc. (Morrisville, PA). HPLC-grade n-heptane and toluene were purchased from Fisher Scientific (Pittsburgh, PA). Absolute ethanol was purchased from Acros Organics (Belgium). All chemicals were used as received. Silicon wafers with [100] orientation were acquired from Silicon Valley Microelectronics (Santa Clara, CA).

Hondo (HOW) crude oil for isolating asphaltenes was obtained from ExxonMobil Upstream Research Company. The lot of Hondo crude used in this study had 14.8% (w/w) asphaltene; the hydrogen to carbon ratio was 1.29. The asphaltene precipitation was described elsewhere.[32] In brief, asphaltenes were obtained by mixing n-heptane and crude oil in a 40:1 volume ratio followed by stirring for 24 hours. The precipitated asphaltenes were removed by vacuum filtration through a 15 cm-diameter Whatman 934-AH glass microfiber filter paper and were sequentially Soxhlet-extracted for 24 hours with n-heptane, to remove residual resins and maltenes, and toluene to re-dissolve the asphaltenes and separate them from carbenes, carboids, and inorganic materials. Toluene was evaporated and the asphaltenes re-dissolved in methylene chloride for transferring. The asphaltenes were finally dried under reduced pressure resulting in a shiny, dark solid.

Sample preparation. Silicon wafers were cut into 1 x 1 cm^2 pieces, cleaned by rinsing with absolute ethanol and exposed to an ultraviolet/ozone (UVO) treatment for 15 minutes. The latter process generates a high density of surface-bound –OH groups needed for attachment of

organosilane SAMs. The cleaned substrates were immediately transferred to a nitrogen-purged glove bag for submersing in deposition solutions.

Stock solutions (2% w/w) of organosilanes were prepared by dissolving the respective trichlorosilanes into HPLC-grade toluene in a nitrogen purged glove bag. These stock solutions were diluted to a final concentration of 2 mmol trichlorosilane per kilogram of solution. Mixed silane solutions were prepared by combining the pure component deposition solutions on a mass basis, for a final trichlorosilane concentration of 2 mmol/kg. The deposition solutions prepared in this manner were used within a day of the time of preparation and only exposed to the atmosphere for the removal of the silicon substrate after deposition. In preliminary experiments we established that asphaltene adsorption varied monotonically with varying the fraction of the aromatic component in the SAM for all combinations of the SAM-forming moieties. In the present work we thus concentrate only on exploring systematically the low (< 0.2) and high (> 0.8) aromatic fraction regimes. Mixed SAMs were formed for mixtures of PTS/BTS, PTS/ODTS, PETS/BTS and PETS/ODTS. Organosilane SAMs were prepared by submersing UVO-treated silicon substrates into deposition solutions of trichlorosilanes in tightly-sealed containers for approximately 16 hours. After SAM formation, the substrates were removed from the deposition solutions and quickly rinsed with toluene and absolute ethanol, followed by drying with nitrogen gas. Replicates of each sample were made in order to 1) establish the properties of the pre- and post- asphaltene treated SAMs, and 2) ensure the reproducibility of the adsorption experiments.

Asphaltene solutions (0.5% w/w) were prepared by dissolving the precipitated, dry asphaltenes in HPLC grade toluene followed by overnight shaking. Asphaltene adsorption was accomplished by exposing the SAM-covered substrates to these solutions for approximately 12

hours. The samples were then rinsed and sonicated in pure toluene for 5 minutes in order to remove any weakly-adsorbed asphaltenic aggregates or precipitated particles. This step was necessary because the substrate surfaces emerged from the toluene solutions with visible particles and stains. This observation is consistent with the aforementioned studies that showed that asphaltenes can adsorb indefinitely to a solid surface in the form of multilayers. As a result of the sonication, the asphaltene layers studied here are relatively thin and involve only irreversibly adsorbed asphaltenic moieties. After sonication, the samples were thoroughly rinsed with toluene and dried with nitrogen gas.

Contact angle measurements. Contact angles (θ) with deionized (DI) water as the probing liquid were measured with a Ramé-Hart contact angle goniometer (model 100-00). Static contact angles were determined after releasing an 8 μL droplet of deionized water on the surface. To measure the advancing and receding contact angles (A-CA and R-CA, respectively), we captured the probing droplet and added (advancing) or removed (receding) 4 μL of DI water. This procedure was repeated for two different spots on each sample and the results were averaged. In our analysis, we assumed that A-CAs provide an estimate of the wettability (*i.e.*, surface energy) of the SAMs. A densely-packed SAM of aliphatic chains should form very hydrophobic surfaces, which exhibit high DI water CAs (θ≈110°). In addition, the contact angle hysteresis (CAH), defined here as the difference between A-CA and R-CA, provides information about the chemical and structural heterogeneities of the SAM. CAH of ≤ 10° is generally considered a signature of a molecularly-uniform surface.[21]

Spectroscopic ellipsometry. Film thickness was determined with a variable angle spectroscopic ellipsometer (VASE) (J.A. Woollam Co.). Ellipsometry measures the difference in the polarization state between the light beams incident and reflected from the surface; it provides

information about the thickness and dielectric properties of the film. Unless otherwise specified, ellipsometric data were collected at an incidence angle of 75° and at wavelengths ranging from 400 to 1100 nm in 10 nm increments.

The ellipsometric angles Ψ and Δ depend on the thickness and dielectric constant of the probed film. While in most cases one can determine the optical constants and thickness from the ellipsometric data, for very thin films, these parameters are highly correlated and cannot be determined simultaneously.[33,34] In order to estimate the thickness of the SAMs, we assumed the value of the index of refraction (n=1.47) and kept it constant through the fitting procedure.[21,35] We note that varying the refractive index of the film by ±0.05 results in an uncertainty of approximately ±1 Å.[36] Even though we cannot determine with complete certainty the exact thickness of the film, the estimated thickness is important for comparison between samples and previously published results.

Near-edge x-ray absorption fine structure (NEXAFS) spectroscopy. NEXAFS data were collected at the NIST/Dow Materials Characterization Facility (beamline U7A) of the National Synchrotron Light Source at Brookhaven National Laboratory (Upton, NY). NEXAFS involves the excitation of core shell electrons by a monochromatic beam of soft x-rays and their subsequent relaxation involving the emission of Auger electrons and fluorescence radiation. The x-ray absorption of thin organic films is preferentially monitored with a partial electron yield (PEY) detector because Auger electron emission represents the dominant relaxation mode for low atomic number atoms, such as carbon.[37] The PEY detector operates at a bias of -150 V in order to detect only electrons that have suffered negligible energy losses, thus enhancing the surface sensitivity of NEXAFS to the uppermost 1-2 nm of the sample.[37,38] NEXAFS derives its elemental specificity from the ability to tune the energy of the incoming synchrotron x-ray beam

to match the excitation energy of the core shell electrons of the element of interest (≈285 eV for carbon, ≈400 eV for nitrogen, ≈535 eV for oxygen). NEXAFS is also sensitive to the chemical environment of the molecules due to the resonance of specific electronic transitions from the core shell levels to unoccupied anti-bonding orbitals. In addition to determining the population of various chemical species on surfaces, NEXAFS is often used to assess the molecular orientation of simple molecules and molecular aggregates present on the surface.[37] In our previous work, we employed NEXAFS to measure the molecular orientation of the aliphatic and aromatic organosilanes used in this study.[31] Here we used NEXFAS to establish the orientation of the fused aromatic rings present in asphaltene films by performing experiments at various x-ray beam-to-sample geometries. No orientation was detected (data not shown), however, indicating that the fused rights did not adopt a preferred orientation in the asphaltene film. All NEXAFS experiments reported here were therefore conducted at the so-called "magic angle", *i.e.*, angle between the sample normal and the electric vector of the x-ray beam equal to 50°, where the PEY intensities are independent of the molecular orientation.[37] The magic angle was chosen to be 50 (rather than customary 54.5°) in order to account for 80% linear polarization of the incident x-ray beam. **Figure 1** depicts typical carbon K-edge NEXAFS spectra for the pure component SAMs. By monitoring the relative intensity of the peaks present in the NEXAFS spectrum one can estimate the population of individual bonds in the SAM. In this work we use the area and position of the peak that corresponds to the $1s \rightarrow \pi^*_{C=C}$ transition (≈285.1 eV) of the NEXAFS spectrum to monitor the aromatic content in the films. The edge jump of the NEXAFS spectra is defined as the difference between the NEXAFS intensities collected at the post-edge (arbitrarily chosen at 320 eV) and the pre-edge (arbitrarily chosen at 280 eV) regions. The edge

jump provides a relative measure of the total amount of carbon present in the specimen. To obtain the $1s \rightarrow \pi^*_{C=C}$ peak areas and the peak position we fit the peak with a Gaussian lineshape.[37] The area of the $1s \rightarrow \pi^*_{C=C}$ peak is taken to be a measure of the net amount of aromatic material probed on the film. The apparent position of the $1s \rightarrow \pi^*_{C=C}$ peak varies depending on the aromatic molecule being probed (**Figure 1** inset). Possible origins of these peak shifts are discussed later in the text. **Figure 2** shows spectra for mixed SAMs (left), asphaltene-treated mixed SAMs (middle), and the difference between these two spectra (right). As will be discussed later in the paper, the changes in the spectral features between these data can be attributed to the variation in the chemical composition of the deposited film, its carbon density, and the total amount of carbon being probed.

Results and Discussion

The advancing contact angles and contact angle hysteresis for the four mixed aromatic/aliphatic SAMs are presented in **Figure 3**. The mixed SAMs exhibit a gradual decrease in the advancing contact angles with increasing aromatic fraction in the SAM deposition solution, indicating that solutions of mixed trichlorosilanes form intermixed SAMs as previously described.[31] ODTS-rich SAMs exhibit the largest A-CA (≈110°), revealing that these SAMs are densely packed and expose a close-packed array of terminal methyl groups to the water droplet. The BTS-rich films exhibit a lower A-CA compared to ODTS-rich SAMs. This observation, consistent with previous results,[35] indicates that these films are less densely packed exposing a substantial fraction of methylene groups and possibly the polar silica substrate to the probing water droplet. Additionally, BTS-rich SAMs exhibit a higher number of structural defects, which might expose

the underlying silica substrate to the probing water droplet, effectively decreasing the A-CA. There are three possible factors contributing to the lower packing densities and therefore the lower A-CAs of BTS SAMs relative to ODTS SAMs. First, the roughness of the silicon substrate, albeit small (≈0.5 nm), may affect the organization of the SAMs. In particular, any step-edge effects that could be present on the surface may influence the organization of the head-groups close to the substrate and hence the molecular packing in the SAMs. Additionally, defects may be present in the in-plane silanol networks in the SAM close to the substrate, which may expose hydroxyl groups on the silica substrate, resulting in lower A-CAs. The impact of these two types of defects on contact angles can be alleviated for longer alkyl mesogen SAMs that experience favorable van der Waals interactions among neighboring molecules that keep them closely-packed. In contrast, shorter mesogens will not be able to closely pack and thus shield the substrate defects effectively. All of these factors are present to varying degrees in all the SAMs studied; their impact decreases with increasing thickness of the SAMs, an observation that will prove important in determining the adsorption of asphaltenes, as will be discussed later in the paper. The SAMs rich in either of the two aromatic molecules (PTS and PETS) exhibit lower A-CA than the aliphatic-rich SAM. The decrease in CA for aromatic SAMs is also a consequence of the SAM exposing the more polar phenyl rings relative to the methyl end-groups in the aliphatic trichlorosilanes to the DI water droplet. The phenyl moieties also pack less densely than ODTS chains, exposing the underlying substrate to the probing liquid and increasing the role of defects in the SAM.

The CAH data plotted in **Figure 3** (open symbols) can be divided in two groups, depending on the aromaticity of the probed film. SAMs rich in the aliphatic component exhibit a lower CAH than SAMs rich in the aromatic component, revealing that the aromatic SAMs

possess a lower packing density and a higher number of defects relative to their aliphatic counterparts. The CAH is indicative of either the chemical or structural heterogeneity of the SAMs. It is thus noteworthy that the CAH does not change markedly (within error) when probing a mixed SAM instead of a pure SAM, suggesting that pure and mixed SAMs exhibit comparable density of chemical and structural heterogeneities.

The ellipsometric thickness of the mixed SAMs as a function of the aromatic fraction in the deposition solution for the four mixed SAM systems under investigation is plotted in **Figure 4**. The thickness of the BTS-based SAMs increases and that of the ODTS-based SAMs decreases with increasing of the aromatic fraction in the deposition solution. This observation provides additional evidence that the composition of the SAMs is comparable to that in the deposition solution. BTS SAMs are the shortest molecules used; they do not form densely-packed SAMs, as suggested by the contact angle data. The PTS-rich and PETS-rich SAMs exhibit comparable thicknesses even though the PETS has two additional methylene spacers between the phenyl group and the silicon atom. This observation is consistent with previous results, which revealed that PTS SAMs form dense films with the phenyl ring oriented perpendicular to the surface while PETS SAMs exist as lower density films with a slightly higher tilt relative to the surface normal.[31] ODTS-rich SAMs exhibit ellipsometric thicknesses consistent with those reported in the literature, indicating that the ODTS chains are in an all-trans configuration and aligned nearly parallel to the surface normal, as confirmed with NEXAFS measurements (not shown here).

The chemical composition and carbon density of the SAMs were characterized using NEXAFS. The aromatic carbon content in the SAMs can be established by monitoring the area under the $1s \rightarrow \pi^*_{C=C}$ peak in the NEXAFS spectra. In **Figure 1** we plot the NEXAFS spectra for

the four types of pure component SAMs. The PTS and PETS spectra feature a pronounced $1s \rightarrow \pi^*_{C=C}$ peak, which represents a surface with high aromatic content. BTS and ODTS SAMs differ in that they exhibit very small, albeit still present, $1s \rightarrow \pi^*_{C=C}$ peaks. Possible sources for the appearance of these peaks in the BTS and ODTS SAM NEXAFS spectra may include the presence of adventitious carbon, beam damage on the sample, and impurities present in the chemicals used for SAM syntheses. Although much care has been taken in this study to minimize the adsorption of atmospheric carbon impurities prior to the NEXAFS experiments by preparing the SAMs immediately prior to each experiment, the specimens are exposed to air after being taken from the deposition solution, dried, and placed in the synchrotron scattering chamber. Some adventitious carbon may thus adsorb on the surface of the samples explaining the small $1s \rightarrow \pi^*_{C=C}$ signal in purely aliphatic SAMs. While an alternative explanation for the presence of small aromatic peaks in the purely aliphatic SAM spectra may, in principle, be attributed to the inclusion of toluene molecules in the SAM matrix, residual toluene in the aliphatic SAMs is likely to be removed during the drying procedure or in the high vacuum environment of the NEXAFS experiment. **Figure 2** shows NEXAFS spectra for mixed SAMs formed from deposition solutions of varying aromatic content (left). The area of the $1s \rightarrow \pi^*_{C=C}$ peak increases with increasing the content of the aromatic component in the deposition solution, indicating that the composition of the SAM mimics very closely that of the deposition solution.

The NEXAFS spectra collected from bare SAM surfaces can be utilized to determine the aromatic content in the SAMs as a function of the aromatic fraction in deposition solution by plotting the $1s \rightarrow \pi^*_{C=C}$ peak area versus the aromatic fraction in deposition solution for all mixed SAMs systems tested (*cf.* **Figure 5**, closed symbols). Note that here the NEXAFS spectra were

not normalized; only the pre-edge (around 280 eV) was brought down to zero; the $1s \rightarrow \pi^*_{C=C}$ peak area thus represents the overall concentration of the aromatic species present in the SAM. One caveat to this approach is associated with the limited probing depth of PEY NEXAFS (< 2 nm). This is particularly relevant to the case of ODTS-based molecules having a large concentration of the C18-alkyls, whose thickness is larger than the probing depth of PEY NEXAFS. The compositions of aliphatic-rich SAMs are very sensitive to changes in the aromatic fraction of the deposition solution. For aliphatic SAMs, the variation in the $1s \rightarrow \pi^*_{C=C}$ peak area appears to be nearly linear with respect to the composition in SAM solution indicating that the aliphatic and aromatic molecules adsorb competitively on the surface. The BTS-based surfaces rich in the aromatic component are not as sensitive as their aliphatic counterparts to changes in the composition of the deposition solution. For SAMs in which BTS is the minority component, the $1s \rightarrow \pi^*_{C=C}$ peak area exhibits little variation with respect to the composition of the deposition solution. This observation implies that for solutions rich in the aromatic component, the aromatic component is faster to populate the surface and that the aromatic content of the SAM is higher than that of the deposition solution. Alternatively, when ODTS is used as the minority component, the compositions of the SAMs retain their sensitivity to changes in the aromatic composition of the deposition solutions, indicating that ODTS SAMs adsorb competitively with the aromatic components and that the composition of the surface resembles closely the composition of the solution. Finally, we note that PTS-based SAMs exhibit, in general, higher $1s \rightarrow \pi^*_{C=C}$ peak areas when compared to the corresponding PETS based SAMs. This supports previous results indicating that PTS forms denser SAMs than PETS.[31]

Subtle changes in the position of any peak in the NEXAFS spectrum relative to the ionization potential (IP) have been associated with the chemical identity of the bonds involved in the NEXAFS resonance and with variations in the bond length.[37,39,40] The aromatic molecules under investigation here exhibit strong $1s \rightarrow \pi^*_{C=C}$ resonances present at photon energies lower than the IP threshold; this facilitates the precise determination of the peak position. **Figure 6** depicts the $1s \rightarrow \pi^*_{C=C}$ peak position as a function of the aromatic fraction of the mixed SAM. We detect a consistent shift in the $1s \rightarrow \pi^*_{C=C}$ peak position that depends sensitively on the aromatic molecule incorporated in the film. For PTS-based mixed SAMs an average of (285.09± 0.01) eV is calculated for the center of the $1s \rightarrow \pi^*_{C=C}$ peak resonance whereas for PETS SAMs the value is (285.26±0.01) eV (*cf.* the inset in **Figure 1**). Furthermore, the $1s \rightarrow \pi^*_{C=C}$ peak center does not vary as a function of aromatic fraction, with the exception of the purely aliphatic samples, suggesting that the $1s \rightarrow \pi^*_{C=C}$ peak position is independent of the concentration of the aromatic moiety on the surface. In the case of a purely-aliphatic SAM, the $1s \rightarrow \pi^*_{C=C}$ resonance peak can be attributed to impurities, adventitious carbon in the film or material produced by beam damage to the sample, and not to an aromatic moiety purposely included in the system. The shift in energy for the aromatic molecules suggests that there is a difference in electronic structure between their carbon-carbon bonds. This may be due to the methylene groups that separate the phenyl ring from the silicon atom in PETS and the differences in the electronic structures of carbon and silicon atoms. Work is currently underway that aims at understanding the nature of the shifts in the $1s \rightarrow \pi^*_{C=C}$ resonance; details will be provided in our future publication.[41]

The adsorption of asphaltenes on the mixed SAMs will be reflected by changes in the positions and intensities of the various NEXAFS peaks and the magnitude of the edge-jump in the NEXAFS spectra. For example, provided that the thickness of the probed film does not surpass the probing depth of PEY NEXAFS (≈1-2 nm), the adsorption of aromatic material on top of the SAMs should be reflected as an increase in the area of the $1s \rightarrow \pi^*_{C=C}$ peak and an increase in the edge-jump signal. **Figure 2** depicts the spectra for mixed SAMs before (left) and after (center) treating with asphaltene solutions and their difference (right). The ODTS spectrum in **Figure 2** exhibits very little variation upon asphaltene adsorption as reflected by the negligible signal seen in the difference spectra, suggesting that very little adsorption of asphaltenes occurred onto the ODTS SAMs. For the more aromatic SAMs (PTS concentration > 15%) the $1s \rightarrow \pi^*_{C=C}$ peak area decreases as a result of the asphaltene adsorption, as evidenced by the presence of pronounced negative peaks in the difference spectra. This indicates that a lower amount of aromatic material is probed after the adsorption of asphaltenes. In addition to changes in peak intensities, the data in **Figure 2** reveal that the spectral edge-jump decreases upon asphaltene adsorption, suggesting a decrease in the amount of carbon probed. This can be explained by 1) considering that asphaltenes possess lower atomic density than the SAMs and 2) the inability of PEY NEXAFS to probe the entire SAM/asphaltene film. The claim that asphaltenes have a lower atomic density relative to a well-packed SAM is supported by neutron scattering data, which reveal that asphaltenic aggregates can incorporate a significant amount of entrained solvent (30-50% v/v).[42,43] When they are adsorbed to SAMs from solution, dried under nitrogen and subsequently exposed to the ultrahigh vacuum of the NEXAFS experiment, the asphaltenic aggregates likely lose a considerable amount of solvent. Because of the presence of

rigid fused aromatic ring complexes, the asphaltenes do not likely collapse upon solvent removal. Instead, they retain a substantial amount of voids, which leads to reducing their atomic density per unit volume. Thus if only the topmost 1-2 nm of the film are probed by PEY NEXAFS and the asphaltene layer has lower atomic density than the SAM, the edge-jump of the NEXAFS spectra would decrease despite the net increase of carbonaceous material on the surface.

In order to better understand the effect of the aromaticity and thickness of the SAM on asphaltene adsorption, in **Figure 5** we plot the $1s \rightarrow \pi^*_{C=C}$ peak area before and after asphaltene adsorption as a function of aromatic fraction in all SAM mixtures studied in this work. For highly aromatic mixed SAMs, the total amount of aromatic carbon probed decreases. In order to correctly interpret this observation one needs to consider the probing depth of the PEY NEXAFS technique, the aromaticity of the adsorbed asphaltene layer, and the total thickness of the combined SAM/asphaltene film. As mentioned previously, the Auger electrons possess a small inelastic mean-free path (<1-2 nm)[38,44] making PEY NEXAFS a very surface-sensitive technique. Although this is beneficial when studying very thin small molecule layers (up to 1 monolayer), it can give rise to difficulties when interpreting PEY NEXAFS data for thicker films. The asphaltene-treated SAMs are likely to be thicker than the probing depth of PEY NEXAFS making it difficult to measure the extent of asphaltene adsorption on the SAMs. In order to draw useful insights from the PEY NEXAFS data, one has to first consider the thickness variation of the asphaltene films resting on top of the SAMs. In **Figure 7** we plot the asphaltene thickness on top of SAMs of various aromaticities for all SAM mixtures studied. The data in **Figure 7** reveal two distinct trends between the aromaticity of the SAM and the thickness of the adsorbed asphaltenes. For ODTS-based SAMs, the asphaltene layer thickness increases with

increasing aromatic character of the SAM. In contrast, for BTS-based SAMs the thickness decreases with increasing aromatic fraction. Given that ODTS-rich SAMs are thicker than BTS based SAMs (*cf.* **Figure 4**), these observations suggest that the extent of asphaltene adsorption depends strongly on the thickness of the SAM as opposed to the aromaticity of the SAM. While detailed discussion of the trends seen in **Figure 7** is presented later in the paper, here we use the differences in the asphaltene thickness variation in the ODTS- and BTS-based systems to correctly interpret the NEXAFS data collected from the asphaltene-coated SAM substrates. In **Figure 5** the $1s \rightarrow \pi^*_{C=C}$ signal intensity is relatively high in asphaltene-treated BTS-based SAMs. Increasing the aromatic content in the SAM does not cause dramatic changes in the $1s \rightarrow \pi^*_{C=C}$ signal intensity. Because the thickness of the asphaltene film under such conditions is much thicker than the probing depth of PEY NEXAFS (*cf.* **Figure 7**), the primary source of the aromatic signal in the PEY NEXAFS reflects the average concentration of the fused rings in the asphaltene layer. With increasing aromaticity of the BTS-based SAMs, the thickness of the asphaltene layer decreases and becomes comparable to the probing depth of PEY NEXAFS. In this regime NEXAFS detects the presence of unsaturated carbon bonds present both in the asphaltenes as well as the underlying SAM. The increase in the $1s \rightarrow \pi^*_{C=C}$ signal can thus be safely attributed to the increased concentration of the phenyl groups in the SAMs. In ODTS SAMs, only a small amount of asphaltene molecules are adsorbed on the surface, as documented by the thin asphaltene thickness presented in **Figure 7**. However, because of the large thickness of the ODTS-rich SAM (*cf.* **Figure 4**), which is larger than the probing depth of PEY NEXAFS, only fused aromatic rings present in the asphaltene layer are detected. Thus in both pure BTS and ODTS SAMs the $1s \rightarrow \pi^*_{C=C}$ signal in PEY NEXAFS originates only from the asphaltene

layer. A further justification for this is provided by comparing the $1s \rightarrow \pi^*_{C=C}$ signal in pure ODTS and BTS SAMs; the former is much smaller than the latter because the thickness of asphaltene on ODTS SAM is much smaller than that on top of BTS SAM (*cf.* **Figure 7**). With increasing the aromaticity of ODTS-based SAMs, the thickness of the mixed SAM layer decreases (*cf.* **Figure 4**) and the thickness of adsorbed asphaltene increases. Both these features contribute to the increase in the $1s \rightarrow \pi^*_{C=C}$ signal in PEY NEXAFS. It is prudent to point out that in all cases, the $1s \rightarrow \pi^*_{C=C}$ signal of pure aromatic SAMs is higher than that of aromatic SAMs coated with asphaltene layer. Considering that the degree of aromaticity of asphaltenes is relatively high, these results reveal that the aromatic carbon density of asphaltene films is lower than those of a densely packed aromatic SAM.

In order to better understand the nature of NEXAFS signals from pure asphaltenes, we spun coated 0.5% (w/w) asphaltene in toluene solutions onto cleaned silicon substrates (for details see Supporting information). Spun-coated asphaltenes on silica show a peak area for the $1s \rightarrow \pi^*_{C=C}$ signal of 0.272 ± 0.002 on the arbitrary unit scale and a peak center of 285.39 eV. This value for the peak area is slightly lower than the signals found for asphaltene-treated aromatic SAMs in **Figure 5**. Assuming that spun-coated asphaltenes have an aromatic content that is similar to that present in asphaltenes passively-adsorbed from solutions, this observation suggests that the carbon in the SAM buried beneath the adsorbed asphaltenes contributes to the overall NEXAFS signal, although its contribution is highly attenuated. Alternatively, asphaltenes of slightly higher aromaticity may be selectively adsorbing to the aromatic-rich SAMs.

Despite the aforementioned limitations of PEY NEXAFS for the study of thick (> 2 nm) films, one can extract important information from the data. It is prudent to mention that a possible method to overcome these limitations is the use of NEXAFS with fluorescence yield (FY) detection whose probing depth is on the order of hundreds of nanometers. While FY NEXAFS appears to be better suited for studying the structure of films thicker than ≈2 nm, the FY of low atomic number atoms upon x-ray absorption is significantly lower than the Auger yield.[37] For this reason FY NEXAFS has lower signal-to-noise ratios when compared to the PEY, and consequently requires longer collection times in order to obtain NEXAFS spectra with good statistics. While we do not employ FY NEXAFS in this study, we utilize it in subsequent work and compare the FY and PEY NEXAFS intensity signal in order to gain more information about the sensitivities of the two detection methods.[41]

The data in **Figure 6** reveal the effect of asphaltene treatment on the position of the $1s \rightarrow \pi^*_{C=C}$ resonance peak (crossed symbols). While the PTS-based SAMs exhibit an increase in the peak position upon asphaltene adsorption at low aromatic fractions, the PETS-based SAMs maintain a constant peak center as a function of the aromatic fraction in the SAM. The shift in the peak position for PTS-based SAMs is attributed to aromatic chemical bonds found in asphaltenic aggregates that have different chemical environments than the trichlorosilane molecules in the SAMs. For primarily aliphatic SAM, the leading contribution to the aromatic PEY signal is due to the aromatic cores in the asphaltenes and not due to the underlying aliphatic SAM. In the case of a primarily aromatic SAM, the predominant aromatic contribution is due to the richly aromatic SAM and not due to the asphaltene signal, resulting in a decrease in the $1s \rightarrow \pi^*_{C=C}$ resonance peak center to the bare monolayer value. While the same effect should be

present in the PETS-based SAMs, it cannot be discriminated in the NEXAFS spectra because the bare PETS has a $1s \rightarrow \pi^*_{C=C}$ peak center similar to those for the adsorbed asphaltenes. Nevertheless, the NEXAFS spectra shown in **Figure 6** demonstrate clearly the power of NEXAFS spectroscopy to discriminate among various chemical functionalities in a thin organic coating.

It is interesting to compare the $1s \rightarrow \pi^*_{C=C}$ peak positions for the asphaltene-treated SAMs to the peak center for the spun-coated asphaltenes. The $1s \rightarrow \pi^*_{C=C}$ peak center in the spun-coated asphaltenes is positioned at 285.39 eV, a value that is higher than all of those observed for the asphaltenes that were passively adsorbed onto the monolayers. One possible reason for this difference is that asphaltenes might interact in a different way with the bare silica, the SAM layers or among themselves. These differences might result in changes to the electronic structure of the molecules and therefore to the shifts observed in the peak positions. An alternative explanation is that the processes by which the asphaltenes are adsorbed in both cases are dissimilar; it is possible that different groups of asphaltenes adsorb on the surface for the two adsorption procedures given the rather chemical heterogeneous nature of asphaltene molecules. The value of 285.39 eV provides a possible explanation for the upturn in peak centers for the aliphatic, asphaltene-treated SAMs.

Earlier in the paper we presented ellipsometric data of the asphaltene-treated samples (*cf.* **Figure 7**). Her we provide more detailed discussion of the data and the trends seen. The data were collected using the same parameters as those described for the bare SAMs. We employ a two-layer model in order to estimate the increase in film thickness due to asphaltene adsorption. The first and second layers resting above the silicon substrate represent the native silica layer and

the SAM, respectively. The SAM layer is modeled as described before; its thickness is fixed to the values reported in **Figure 4**. The second layer, comprising adsorbed asphaltenes, is modeled by assuming an index of refraction of 1.8, a number obtained from measuring the refractive index of spun-coated asphaltene on silicon substrates. Determining the refractive index of spun-coated asphaltenes from ellipsometry is possible because the thickness of these films is high enough so that the thickness and refractive index of the film are no longer correlated. The value of 1.8 determined with this method is higher than refractive index values estimated routinely for asphaltenes in solution.[45] The difference might be attributed to the difference in structure of the asphaltenic molecules in the adsorbed layer (relative to solution state) and possible chemical fractionation of the asphaltenes upon adsorption. Experimental studies reported that molecules with fused polyaromatic rings might reach refractive indexes ≈2.2.[46] Assuming that typical aliphatic hydrocabons have refractive indices around 1.43, taking the value of the refractive index for aromatic fused rings to be ≈2.2, and considering that the aromatic and aliphatic fractions of asphaltenes are 0.6 and 0.4 respectively; one can estimate the effective refractive index of an asphaltene layer to be n_{theo}>1.9. This value is higher than the value of 1.8 measured experimentally in this work. A possible explanation for n_{exp} (=1.8) < n_{theo} is that the adsorbed asphaltene layer contains voids, which would cause the observed decrease in the refractive index of asphaltene relative to densely packed fused polyaromatic rings. This explanation is consistent with the NEXAFS experiments discussed earlier, and while it still needs to be validated by additional experiments, this approach provides a convenient means of approximating relative changes in the asphaltene thickness from sample to sample.

The thickness of the asphaltene layer as a function of the aromatic mole fraction in deposition solution is plotted in **Figure 7** for two separate sets of experiments. The comparison

of the two data sets provides insight into the reproducibility of our experiments. Although the trend in the adsorption of asphaltenes is consistent between the two sets the absolute values of the adsorbed thickness differ slightly. Among the factors contributing to this lack of absolute reproducibility are: 1) the chemical amphiphilicity and structural heterogeneity of asphaltenes, 2) the overall properties of the SAMs, 3) the sonication procedure, 4) and traces of water that may be present both in the solvent and during the SAM deposition. The SAM quality has a pronounced effect on both the trends and the absolute extent of asphaltene adsorption. In a separate set of experiments (unpublished data) we observed that adsorption of asphaltenes on the SAM monolayer, in cases in which the SAM had lower hydrophobicity, resulted in irreproducible adsorption data. Another factor possibly contributing to the data scatter is that a different sonicating bath had to be used for the different experimental sets, which will lead to different amounts of asphaltenes being removed from the surface depending on the sonication power of the specific instrument.[2] For this reason, data comparisons should be made among data points collected in the same data set.

As discussed earlier in the paper, BTS- and ODTS-based SAMs exhibit opposite trends as the aromaticity of the SAMs increases. Specifically, the asphaltene adsorption on BTS based SAMs decreases with increasing aromaticity whereas for ODTS SAMs the asphaltene adsorption increases with increasing aromaticities. This observation suggests strongly that the extent of asphaltene adsorption depends on the thickness of the underlying SAM. In **Figure 8** we plot the thickness of the asphaltene layer as a function of the SAM thickness. Based on the data in **Figure 8** one can conclude that the thickness of the asphaltene layer decreases with increasing SAM thickness. It is possible to divide the data into three distinct groups depending on the majority component of the SAM. BTS-rich SAMs represent the thinnest SAMs; they exhibit the

largest amounts of asphaltene adsorption. The BTS-rich SAMs are closely followed by the aromatic-rich SAMs. PTS and PETS SAMs have equivalent thicknesses (*cf.* **Figure 4**) resulting in little difference in the extent of asphaltene adsorption between these films. This observation is consistent with the similar attenuations of the $1s \rightarrow \pi^*_{C=C}$ peak areas for SAMs rich in the aromatic component after asphaltene deposition (*cf.* **Figure 5**). The lowest asphaltene adsorption is detected on ODTS-rich SAMs, the thickest, densest and most hydrophobic SAMs studied. The fact that the asphaltene thickness depends on the thickness of the SAMs suggests that the leading interaction affecting asphaltene adsorption onto SAMs is the interaction with the underlying SiO_x substrate rather than the interaction between asphaltenes and the tail group in the SAM. We note that interaction of polar groups with the underlying silica substrate across a thin hydrophobic SAM layer has recently been reported by Semler and coworkers.[47] In addition, given the limitations one faces in preparing "perfect" defect-free SAM layers it is very likely that there is a population of defects in which silanol groups in the underlying silica are occasionally exposed. These act as attraction sites for possible interaction with polar groups present in asphaltenes. The role of defects, *i.e.*, silica step-edges and substrate roughness, in-plane defects in the network of Si-O bonds of the SAM and the reduced coherence of the SAMs due to incorporation of varying chemical moieties, on the adsorption of asphaltenes decreases for thicker SAMs because the long alkane mesogens will effectively shield any interaction between the asphaltenes and the underlying silica substrates (even if defects are present close to the head-group) resulting in lower amounts of adsorbed asphaltene. For thin SAM films however, there are no long chemical moieties able to shield the interactions at defect sites, resulting in higher amounts of adsorbed asphaltenes. Even though our original hypothesis was that the asphaltenes would interact strongly with an aromatic surface, it is not surprising that the strongest interaction

is with the high energy silica substrate. Asphaltenes constitute some of the most polar components in crude oil and they can therefore interact strongly with the underlying polar SiO_x substrate through the polar moieties present in asphaltenes, viz. pyridinic and pyrollic nitrogen, phenolic hydroxyl, carboxylic groups, and quinonic oxygen. The aromaticity of the SAMs seems to play a minor role in the adsorption process.

Conclusions

We have studied the adsorption of asphaltenic aggregates on SAMs of fine-tuned aromatic/aliphatic composition. Our results reveal that good control of the SAM composition can be achieved by carefully varying the ratio of the aromatic to aliphatic organosilanes in the deposition solution. The asphaltene adsorption experiments show that the aromaticity of the SAM is not the leading factor in determining adsorption of asphaltenes. Instead, we observed that the ability of the SAM to shield the polar SiO_x substrate is the most significant factor in determining the extent of asphaltene adsorption. We used PEY NEXAFS as a tool to study the adsorption of asphaltenes. We note that PEY has some limitations when dealing with adsorption studies that involve films that are thicker that the inelastic mean free path of Auger electrons. A way to overcome these limitations is to use fluorescence yield NEXAFS for absolute characterization of the adsorption events and comparison to the ellipsometry data. Experiments employing both PEY and FY NEXAFS signals will be reported in a subsequent publication.[41]

Acknowledgments

NEXAFS spectroscopy experiments were carried out at the National Synchrotron Light Source, Brookhaven National Laboratory, which is supported by the U.S. Department of Energy,

Division of Materials Sciences and Division of Chemical Sciences. Certian commercial names are mentioned in this manuscript, this does not constitute an endorsement by the National Institute of Standards and Technology.

Supporting Information

Supporting Information Available: The preparation and characterization of spun-coated asphaltenes including ellipsometry and NEXAFS data is available as supporting information. This material is available free of charge via the Internet at http://pubs.acs.org.

References

(1) Leontaritis, K. J.; Mansoori, G. A. *J. Pet. Sci. Eng.* **1988***, 1*, 229-239.

(2) Sheu, E. Y.; Mullins, O. C., Eds.; In *Asphaltenes: fundamentals and applications;* Plenum Press: New York, 1995; pp 245.

(3) Thawer, R.; Nicoll, D. C. A.; Dick, G. *SPE Prod. Eng.* **1990***, 5*, 475-480.

(4) Misra, S.; Baruah, S.; Singh, K. *SPE Prod. Facil.* **1995***, 10*, 50-54.

(5) Mansoori, G. A. In Proceedings of the 9th International Conference on Properties and Phase Equilibria for Product and Process Design; 2001.

(6) Dudášová, D.; Silset, A.; Sjöblom, J. *J. Dispersion Sci. Technol.* **2008***, 29*, 139-146.

(7) Abdallah, W. A.; Taylor, S. D. *Nucl. Instrum. Methods Phys. Res. Sect. B* **2007***, 258*, 213-217.

(8) Acevedo, S.; Ranaudo, M. A.; Garcia, C.; Castillo, J.; Fernandez, A. *Energy Fuels* **2003***, 17*, 257-261.

(9) Xie, K.; Karan, K. *Energy Fuels* **2005***, 19*, 1252-1260.

(10) Speight, J. G. In *The Chemistry and Technology of Petroleum;* Chemical Industries; Marcel Dekker, Inc.: New York, 1999; Vol. 76, p 918.

(11) Drummond, C.; Israelachvili, J. *J. Pet. Sci. Eng.* **2004***, 45*, 61-81.

(12) Toulhoat, H.; Prayer, C.; Rouquet, G. *Colloids Surf. , A* **1994***, 91*, 267-283.

(13) Batina, N.; Manzano-Martinez, J. C.; Andersen, S. I.; Lira-Galeana, C. *Energy Fuels* **2003***, 17*, 532-542.

(14) Batina, N.; Reyna-Cordova, A.; Trinidad-Reyes, Y.; Quintana-Garcia, M.; Buenrostro-Gonzalez, E.; Lira-Galeana, C.; Andersen, S. I. *Energy Fuels* **2005***, 19*, 2001-2005.

(15) Castillo, J.; Goncalves, S.; Fernández, A.; Mujica, V. *Opt. Commun.* **1998***, 145*, 69-75.

(16) Acevedo, S.; Castillo, J.; Fernandez, A.; Goncalves, S.; Ranaudo, M. A. *Energy Fuels* **1998***, 12*, 386-390.

(17) Acevedo, S.; Ranaudo, M. A.; Garcia, C.; Castillo, J.; Fernandez, A.; Caetano, M.; Goncalvez, S. *Colloids Surf. , A* **2000***, 166*, 145-152.

(18) Ekholm, P.; Blomberg, E.; Claesson, P.; Auflem, I. H.; Sjöblom, J.; Kornfeldt, A. *J. Colloid Interface Sci.* **2002***, 247*, 342-350.

(19) Labrador, H.; Fernandez, Y.; Tovar, J.; Munoz, R.; Pereira, J. C. *Energy Fuels* **2007***, 21*, 1226-1230.

(20) Hannisdal, A.; Ese, M.; Hemmingsen, P. V.; Sjöblom, J. *Colloids Surf. , A* **2006***, 276*, 45-58.

(21) Ulman, A. In *An introduction to ultrathin organic films : from Langmuir-Blodgett to self-assembly;* Academic Press: Boston, 1991; p 442.

(22) Sagiv, J. *J. Am. Chem. Soc.* **1980***, 102*, 92-98.

(23) Netzer, L.; Sagiv, J. *J. Am. Chem. Soc.* **1983***, 105*, 674-676.

(24) Netzer, L.; Iscovici, R.; Sagiv, J. *Thin Solid Films* **1983***, 99*, 235-241.

(25) Netzer, L.; Iscovici, R.; Sagiv, J. *Thin Solid Films* **1983***, 100*, 67-76.

(26) Maoz, R.; Sagiv, J. *J. Colloid Interface Sci.* **1984***, 100*, 465-496.

(27) Gun, J.; Iscovici, R.; Sagiv, J. *J. Colloid Interface Sci.* **1984***, 101*, 201-213.

(28) Gun, J.; Sagiv, J. *J. Colloid Interface Sci.* **1986***, 112*, 457-472.

(29) Finklea, H. O.; Robinson, L. R.; Blackburn, A.; Richter, B.; Allara, D.; Bright, T. *Langmuir* **1986***, 2*, 239-244.

(30) Allara, D. L.; Parikh, A. N.; Rondelez, F. *Langmuir* **1995***, 11*, 2357-2360.

(31) Smith, M. B.; Efimenko, K.; Fischer, D. A.; Lappi, S. E.; Kilpatrick, P. K.; Genzer, J. *Langmuir* **2007***, 23*, 673-683.

(32) Spiecker, P. M.; Gawrys, K. L.; Kilpatrick, P. K. *J. Colloid Interface Sci.* **2003***, 267*, 178-193.

(33) McCrackin, F. L.; Passaglia, E.; Stromberg, R. R.; Steinberg, H. L. *J. Res. Natl. Bur. Stand. Sect. A* **1963***, A 67*, 363-377.

(34) McCrackin, F. L.; Passaglia, E.; Stromberg, R. R.; Steinberg, H. L. *J. Res. Nat. Inst. Stand. Technol.* **2001***, 106*, 589-603.

(35) Wasserman, S. R.; Tao, Y. T.; Whitesides, G. M. *Langmuir* **1989***, 5*, 1074-1087.

(36) Tillman, N.; Ulman, A.; Schildkraut, J. S.; Penner, T. L. *J. Am. Chem. Soc.* **1988***, 110*, 6136-6144.

(37) Stöhr, J. In *NEXAFS Spectroscopy;* Springer Series in Surface Sciences 25; Springer-Verlag: New York, 1992; p 403.

(38) Genzer, J.; Kramer, E. J.; Fischer, D. A. *J. Appl. Phys.* **2002***, 92*, 7070-7079.

(39) Sette, F.; Stohr, J.; Hitchcock, A. P. *J. Chem. Phys.* **1984***, 81*, 4906-4914.

(40) Sette, F.; Stohr, J.; Hitchcock, A. P. *Chem. Phys. Lett.* **1984**, *110*, 517-520.

(41) Turgman-Cohen, S.; Fischer, D. A.; Kilpatrick, P. K.; Genzer, J. In preparation.

(42) Gawrys, K. L.; Kilpatrick, P. K. *J. Colloid Interface Sci.* **2005**, *288*, 325-334.

(43) Gawrys, K. L.; Blankenship, G. A.; Kilpatrick, P. K. *Langmuir* **2006**, *22*, 4487-4497.

(44) Sohn, K. E.; Dimitriou, J.; Genzer, J.; Fischer, D. A.; Hawker, C. J.; Kramer, E. J. Submitted.

(45) Buckley, J. S.; Hirasaki, G. J.; Liu, Y.; Von Drasek, S.; Wang, J. X.; Gil, B. S. *Petrol. Sci. Technol.* **1998**, *16*, 251-285.

(46) McCartney, J. T.; Ergun, S. *J. Opt. Soc. Am.* **1962**, *52*, 197-200.

(47) Semler, J. J.; Jhon, Y. K.; Tonelli, A.; Beevers, M.; Krishnamoorti, R.; Genzer, J. *Adv. Mater.* **2007**, *19*, 2877-2883.

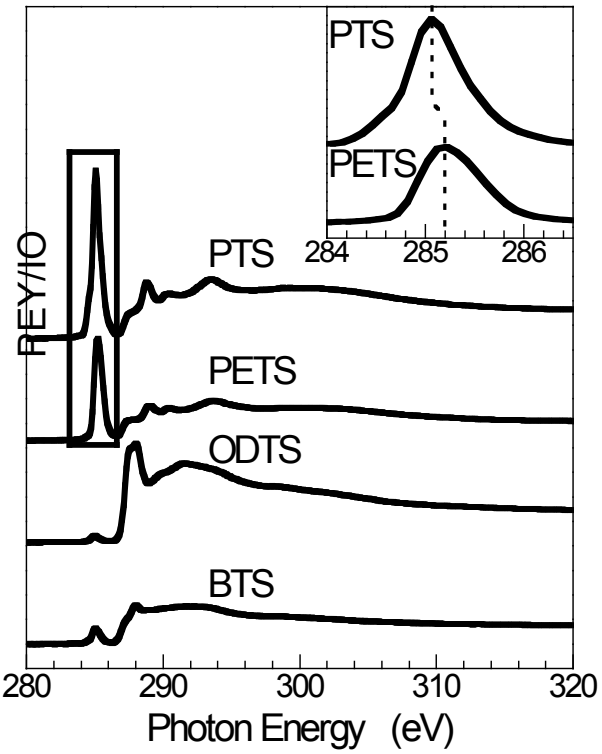

Figure 1. PEY NEXAFS spectra collected at the carbon K-edge at the "magic" angle of incidence (θ=50°, where θ is the angle between the sample normal and the electric vector of the x-ray beam) for the pure component trichlorosilane SAMs. The inset depicts a shift of ≈0.15 eV between the $1s \rightarrow \pi^*_{C=C}$ peak positions in the NEXAFS spectra of the PTS and PETS SAMs.

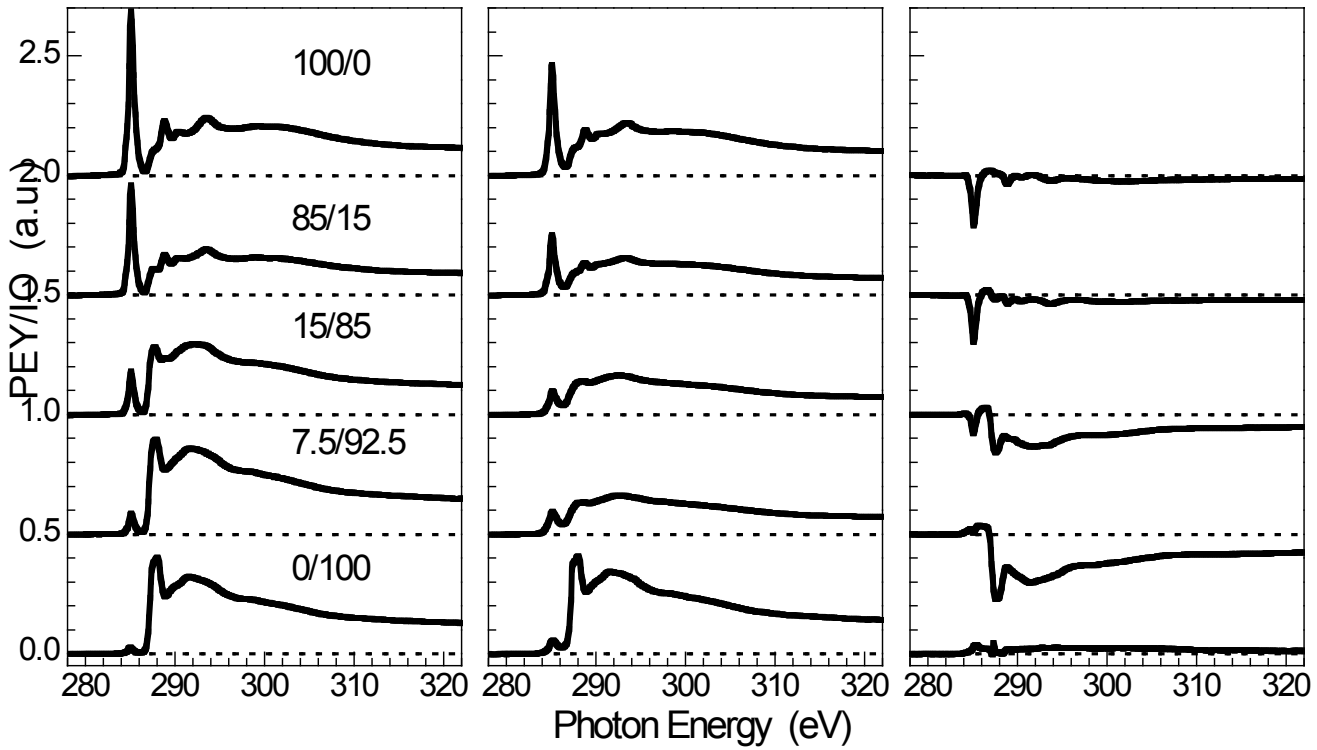

Figure 2. NEXAFS spectra collected at the carbon K-edge for mixed SAMs (left), asphaltene-treated mixed SAMs (center), and the difference between these two spectra (right). The sample compositions (percentage PTS/percentage ODTS) in the PTS/ODTS SAM correspond (from top to bottom) to 100/0, 85/15, 15/85, 7.5/92.5, and 0/100.

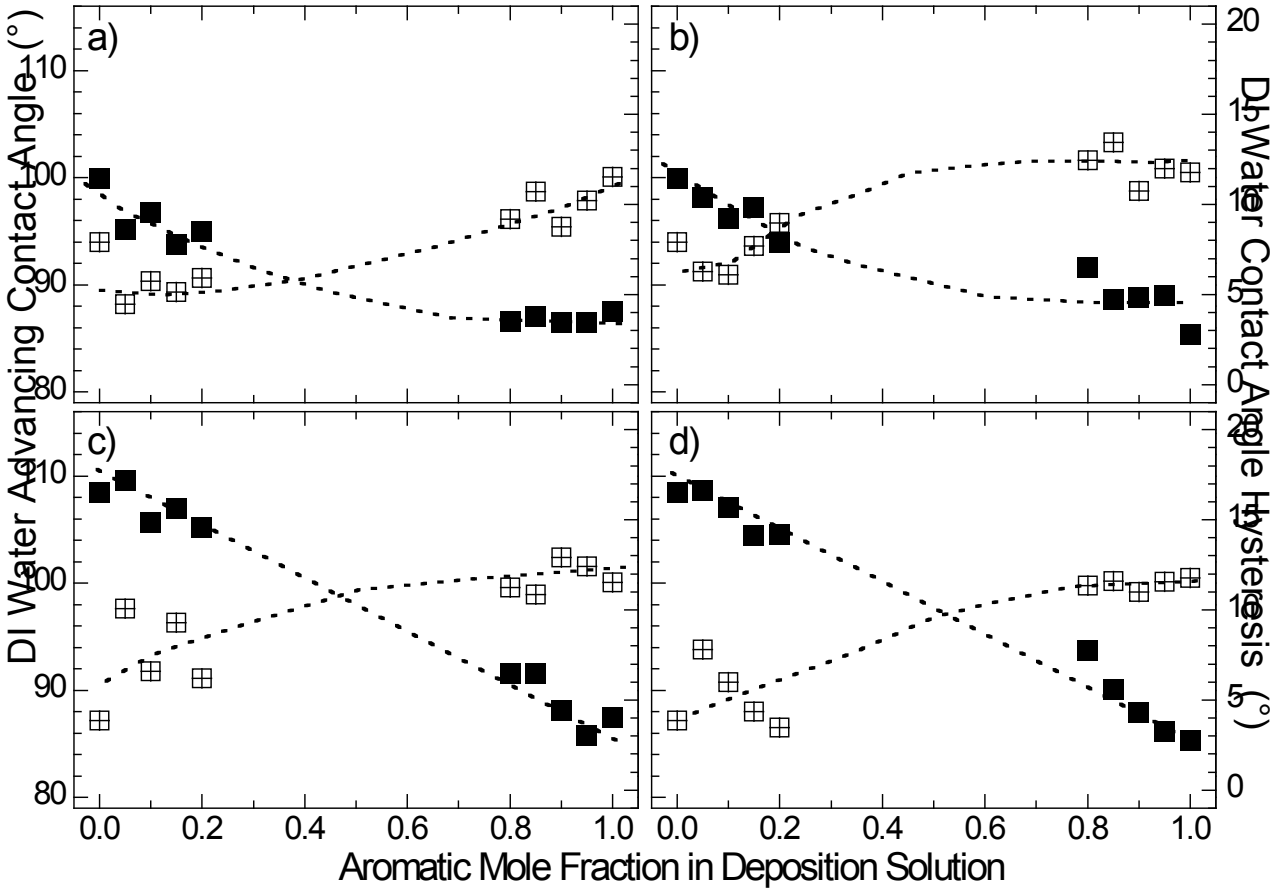

Figure 3. Advancing contact angle (■, left ordinate) and contact angle hysteresis (⊞, right ordinate) as a function of aromatic fraction in deposition solution for: a) PTS:BTS, b) PETS:BTS, c) PTS:ODTS, and d) PETS:ODTS. The error bars are smaller than the sizes of the symbols. The lines are meant to guide the eye.

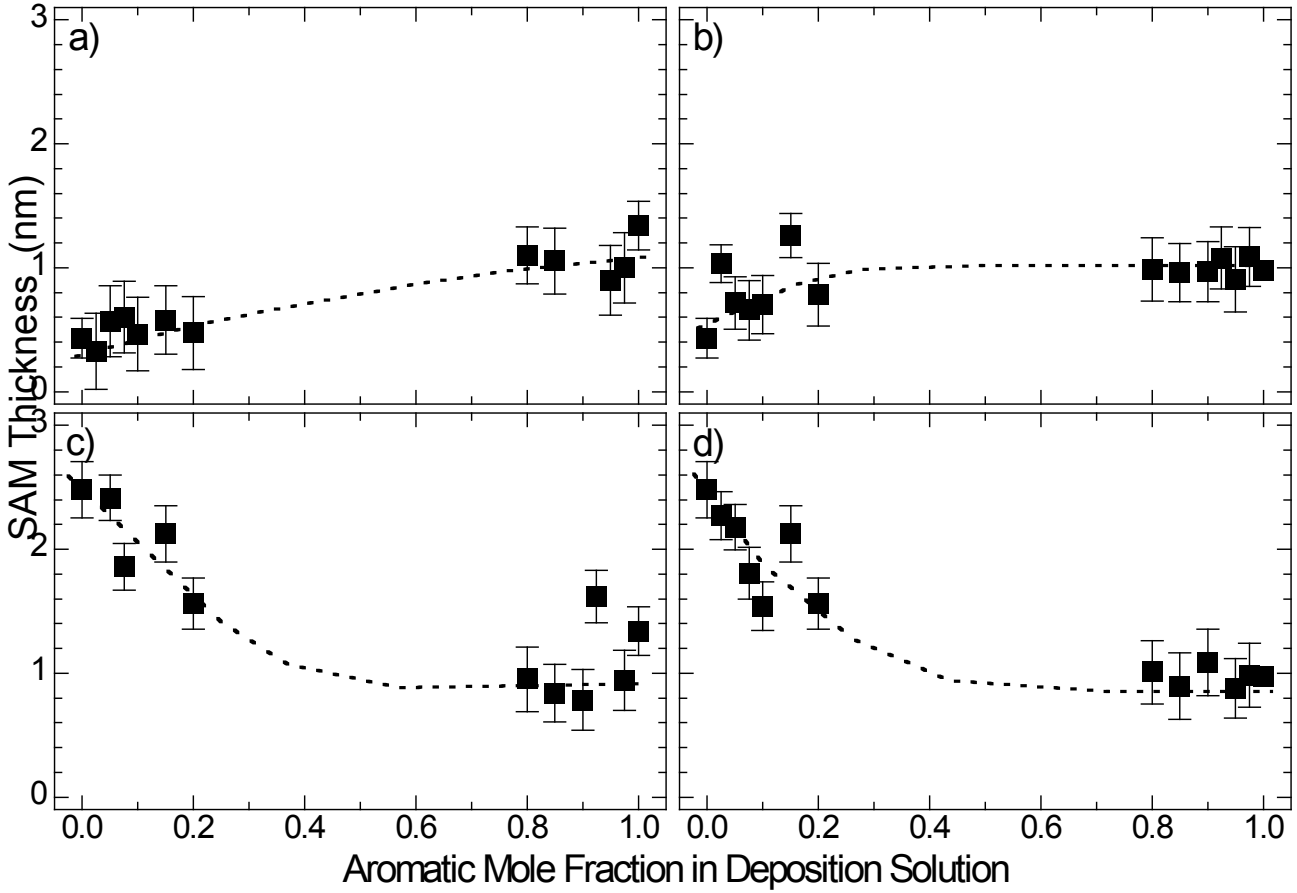

Figure 4. SAM thickness as a function of aromatic mole fraction in the deposition solution for a) PTS:BTS, b) PETS:BTS, c) PTS:ODTS, and d) PETS:ODTS. The lines are meant to guide the eye.

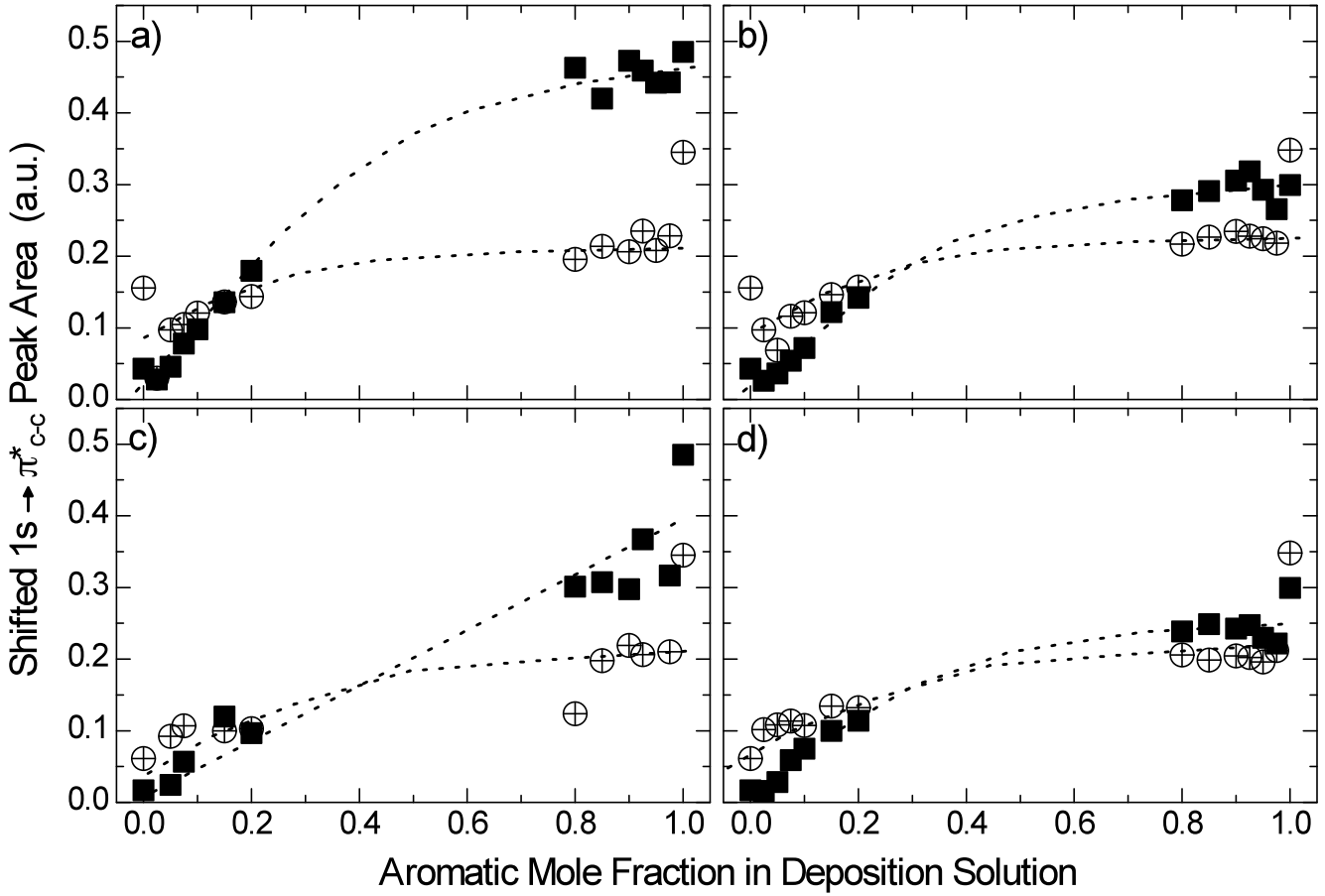

Figure 5. $1s \rightarrow \pi^*_{C=C}$ peak area in the carbon K-edge NEXAFS spectra as a function of aromatic mole fraction in the deposition solution for bare SAMs (■) and HOW asphaltene-treated SAMs (⊖) for a) PTS:BTS, b) PETS:BTS, c) PTS:ODTS, and d) PETS:ODTS. The lines are meant to guide the eye.

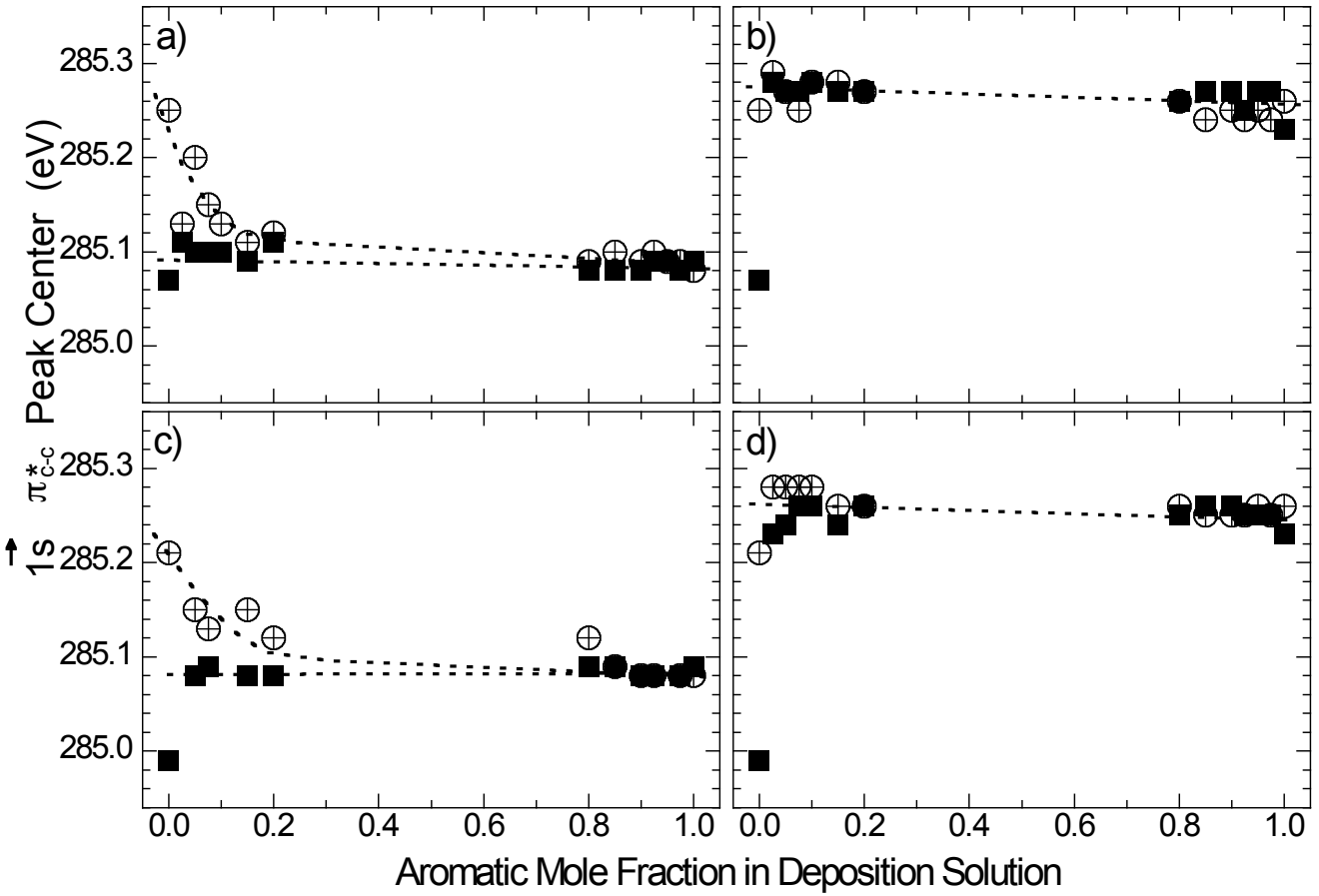

Figure 6. The $1s \rightarrow \pi^*_{C=C}$ peak position in the carbon K-edge NEXAFS spectra as a function of aromatic mole fraction in the deposition solution for bare SAMs (■) and HOW asphaltene-treated SAMs (⊖) for a) PTS:BTS, b) PETS:BTS, c) PTS:ODTS, and d) PETS:ODTS. The lines are meant to guide the eye.

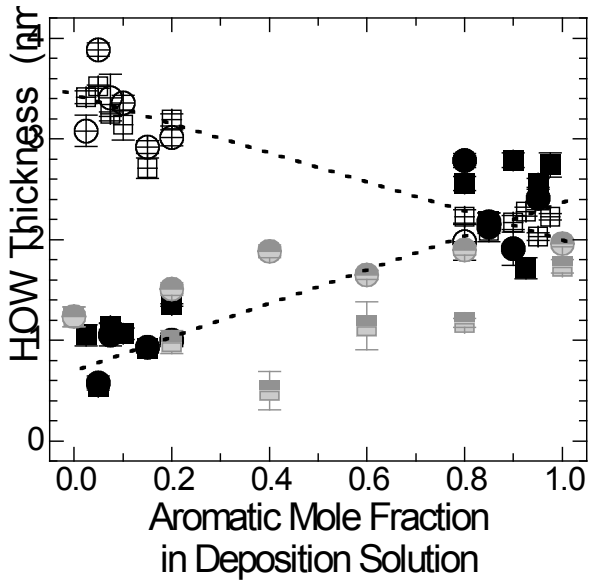

Figure 7. The thickness of the adsorbed asphaltene film determined by ellipsometry as a function of aromatic fraction in the deposition solution for PTS:BTS (⊠), PETS:BTS (⊖), PTS:ODTS (■) and PETS:ODTS (●) mixed SAMs. The grey symbols represent repeat experiments for PTS:ODTS (squares) and PETS:ODTS (circles). The lines are meant to guide the eye.

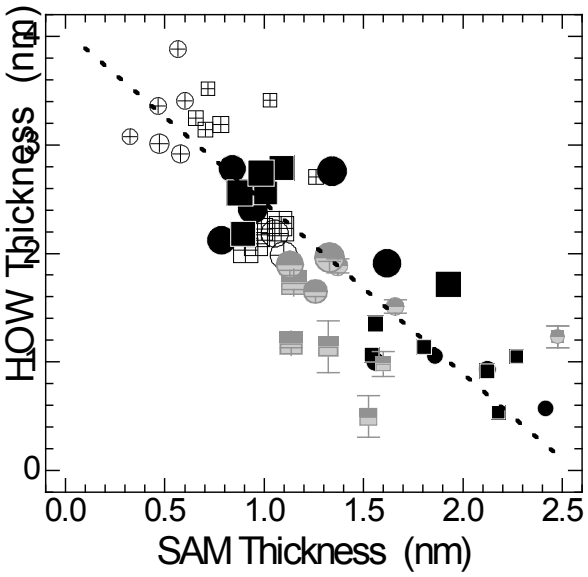

Figure 8. The asphaltene film thickness plotted as a function of the thickness of the underlying SAM for PTS:BTS (⊠), PETS:BTS (⊖), PTS:ODTS (■) and PETS:ODTS (●). The marker size represents the degree of aromaticity (increasing marker size corresponds to increasing degree of aromaticity) of a given data point. The size of each symbol increases proportionally with increasing aromaticity of the SAM solution. The grey symbols represent repeat experiments for PTS:ODTS (squares) and PETS:ODTS (circles). The line is meant to guide the eye.

For Table of Content Use Only

Asphaltene Adsorption onto Self-Assembled Monolayers of Mixed Aromatic and Aliphatic Trichlorosilanes

Salomon Turgman-Cohen, Matthew B. Smith, Daniel A. Fischer, Peter K. Kilpatrick, Jan Genzer

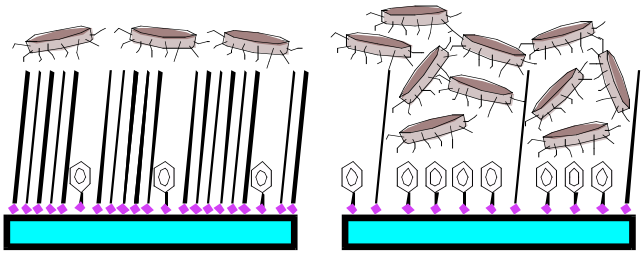

Schematics depicting the adsorption of asphaltenes on top of mixed SAMs composed of various fractions of long alkyl and short phenyl-based organosilanes.